Spin distribution of the compound nucleus formed by $^{16}O + ^{154}Sm$

S. Gil,* R. Vandenbosch, A. Charlop, A. García, D. D. Leach, S. J. Luke, and S. Kailas†

University of Washington, Seattle, Washington 98195

(Received 24 September 1990)

Gamma-ray multiplicities for the $^{16}O + ^{154}Sm$ system have been determined using two different coincidence techniques. Fusion events are tagged either by observation of low-lying gamma transitions in the evaporation residues or by direct detection of the residues exploiting an electrostatic deflector and time-of-flight identification. The gamma-ray tagging measurements have been made with higher sensitivity than previously, allowing us to include the contribution of the $3n$ channel. The contribution of this channel modifies the conclusions made before in regard to the spin distribution of the compound nucleus produced at near-barrier energies. The procedure for conversion of gamma-ray multiplicities to mean spin values has been calibrated by measuring gamma-ray multiplicities and fusion cross sections for the $^4He + ^{166}Er$ and $^3He + ^{167}Er$ reactions that lead to the same compound nucleus as $^{16}O + ^{154}Sm$, at bombarding energies that span the same region of excitation energies and spin. The use of an electrostatic deflector enables an inclusive tag on all evaporation residues, and has sufficient sensitivity to enable measurements at a lower energy than is possible with gamma-ray tagging techniques. The energy dependence of the mean spin deduced from gamma-ray multiplicity measurements is in qualitative agreement with model calculations which include the effects of the static and dynamical deformations of the target nucleus. There is, however, a tendency for the calculations to underestimate somewhat the mean spin near and below the barrier.

I. INTRODUCTION

Several experiments at near-barrier energies have found spin distributions of the compound nucleus which are broader than those expected from theoretical models, even when these models seem to successfully reproduce the excitation functions for the fusion cross section σ_{fus}.[1,2]

In a previous gamma-ray multiplicity study of the first moment of the spin distribution, $\langle \ell \rangle$, in the system $^{16}O + ^{154}Sm$ at near-barrier energies, we found that σ_{fus} and $\langle \ell \rangle$ could be accounted for by using a one-dimensional penetration model including the target deformation.[3] The technique used in the determination of the gamma-ray multiplicity M_γ relied upon tagging evaporation residues by the detection of discrete gamma rays emitted by the evaporation residues. Due to light-element contaminants in the target and to the complex character of the gamma decay of even-odd nuclei, we were only able to obtain the contribution to M_γ from the $4n$ channel (^{166}Yb) in our earlier study. Near and below the barrier the $3n$ channel begins to make a sizable contribution[4] and its inclusion may significantly modify the conclusions reached before.

In the present work we have investigated this issue by using a new ^{154}Sm target in which oxygen and other low-Z contaminants were minimized. We have been able to clearly identify the gamma rays arising from the $3n$ channel (^{167}Yb). In particular, we were able to observe the transitions originating in the decay through the yrast band (based on the state $\frac{5}{2}^+$[642]). The $E_\gamma = 221.7$ keV

($\frac{17}{2}^+ \rightarrow \frac{13}{2}^+$) transition of this band was used to tag the $3n$ channel.

The technique used for obtaining the contribution of the $3n$ channel $[M_\gamma(3n)]$ to the total M_γ selectively samples those states in the compound nucleus that feed the state $J = \frac{17}{2}^+$ in ^{167}Yb. Similarly the contribution from the $4n$ channel, tagged by the $4^+ \rightarrow 2^+$ transition, samples those states which feed this transition. In order to eliminate the bias produced by this effect, corrections were made using results from statistical decay models. The parameters of the model were adjusted so as to reproduce the relative yield of the different xn channels in the same system.[4]

We deduce the values of $\langle \ell \rangle$ from the measured multiplicities. In order to test the reliability of the deduction of $\langle \ell \rangle$ we have also measured M_γ and σ_{fus} for the systems $^4He + ^{166}Er$ and $^3He + ^{167}Er$ that lead to the same compound nucleus as $^{16}O + ^{154}Sm$ (^{170}Yb). The compound nuclei produced in these reactions span the same region of excitation energy and spin as the reaction $^{16}O + ^{154}Sm$ at near-barrier energies. Since for more asymmetric systems at energies above the barrier predictions of the spin distribution can be safely made,[3] these reactions become natural benchmarks for testing the procedure of converting M_γ into $\langle \ell \rangle$.

In an effort to develop a new technique that would allow us to explore the spin distribution at energies as far below the barrier as possible, we have devised a new technique to measure M_γ using an electrostatic deflector. Since the fusion products are strongly peaked at 0°,

large detection efficiency can be achieved if it is possible to separate and suppress the beamlike particles from the fusion products. Furthermore, by using directly the fusion products as a tag for the fusion process, the effect of channel fractionation can be eliminated.

II. EXPERIMENT

The fusion cross sections and the gamma-ray multiplicities have been measured for the ^{4}He+^{166}Er, ^{3}He+^{167}Er, and ^{16}O+^{154}Sm systems. The ^{16}O and ^{3}He beams were provided by the University of Washington FN tandem. The ^{4}He beam at energies above 27.5 MeV was obtained using the new superconducting booster following the tandem. The ^{154}Sm target was a self-supporting, 98.7% enriched, of 450 μg/cm^2. This target was produced by the Oak Ridge National Laboratory using a special technique that minimizes oxygen and other low-Z contaminants. The ^{166}Er target was 155 μg/cm^2 thick, 96% enriched, evaporated on a 30-μg/cm^2 carbon backing. The ^{167}Er target was made of ^{167}ErO$_2$, 62% enriched isotope, painted on a 100-μg/cm^2 carbon backing, of about 1 mg/cm^2.

Our experimental method made use of two experimental setups. The first setup was devised to determine the fusion cross sections and the gamma multiplicities, using a discrete gamma-ray technique, similar to the one used in Ref. 3. The second setup employed an electrostatic deflector and a recoil detector as a fusion tag.

The first setup consisted of a 50-cm^3 GeLi detector placed at 90° with respect to the beam and at 4 cm from the target. Two 7.6×7.6-cm NaI detectors were placed at 55° and 125° with respect to the beam and at 19.4 cm from the target. A 0.965-mm-thick copper and a 1.75-mm lead absorber were placed in front of each NaI detector. A particle monitor detector was placed at 30° for absolute normalization. These absolute normalizations were also checked against the beam integrated charge in the Faraday cup. The variation of the beam intensity was recorded by multiscaling the Faraday-cup charge in 20-sec intervals. The efficiencies of the gamma-ray detectors were obtained by placing calibrated sources at the target position. Bombarding energies were corrected to the average midpoint energy in the target.

A. Determination of the fusion cross sections

The fusion cross section for the ^{16}O+^{154}Sm reaction was measured by Stokstad *et al.*[4] For the ^{3}He and ^{4}He systems, the fusion cross sections were obtained by adding the contribution of the $2n$, $3n$, and $4n$ residue evaporation channels. The fusion cross sections for the $2n$ and $4n$ channels were deduced from the intensities of the gamma rays deexciting the ground-state rotational band. The lowest observable transition is the 4^+ to 2^+ transition, as the 2^+ to 0^+ transition is highly converted. The channel yield was deduced from an extrapolation of the rotational transition intensities to $I = 0$. This technique is the same as was used in Ref. 5 for determining evaporation residue cross sections. Some examples of this

extrapolation are shown in Fig. 1. For the ^{4}He-induced reaction the extrapolated cross section was of the order of 30% larger than the observed 4^+ to 2^+ cross section, whereas for the ^{3}He-induced reaction the extrapolated cross section was a factor of 2 higher, leading in the latter case to a significant uncertainty in the $2n$ and $4n$ channel yields.

The $3n$ channel was determined by an activation technique. The target was irradiated for typically 20 min. A 100-μg/cm^2 carbon foil placed immediately after the target was used as a catcher for the evaporation residues. After irradiation the radioactivity of 17-min ^{167}Yb was observed using the 106-, 113-, and 176-keV gammas. The absolute cross sections are based primarily on the stronger 113-keV line, for which there are 0.55 photon per disintegration. Corrections were made for decay during bombardment and prior to and during the counting interval. Variation of the beam intensity during the irradiation was also taken into account. The results of these measurements are summarized in Table I. The indicated errors include uncertainties in the target thickness, detection efficiency, and (in the case of the $2n$ and $4n$ channels) the extrapolated cross section. Also shown are the $\langle \ell \rangle$ values deduced from the measured cross sections using the sharp-cutoff approximation and using spin distributions taking into account the target deformation. The latter values were obtained using the Wong model or a coupled-channels calculation, and differ little from the sharp-cutoff approximation for these above-barrier energies.

B. Gamma-ray multiplicities

The measurements of M_γ were made using two different techniques. The first employed tagging on discrete
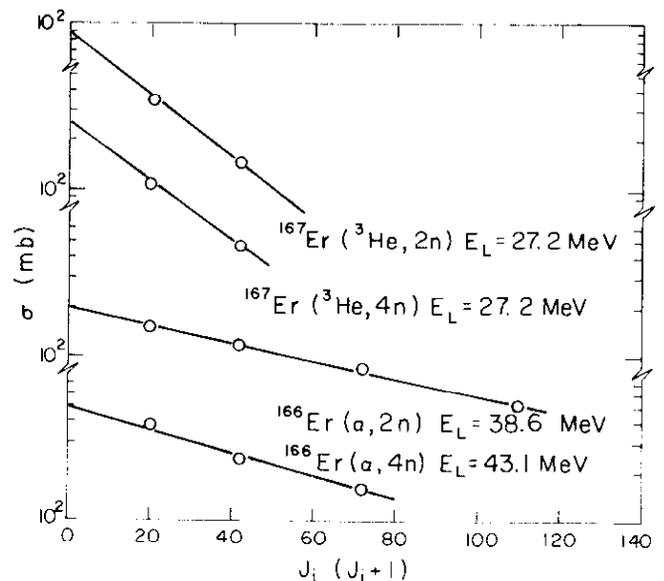

FIG. 1. Samples of transition cross sections for the ground-state rotational band transitions $J \rightarrow J - 2$ vs $J^*(J + 1)$ for the various calibration reactions.

TABLE I. Evaporation residue cross sections measured in this work. The last column gives the $\langle \ell \rangle$ values derived from the sharp-cutoff model and in the case of $^3\text{He}+^{167}\text{Er}$ include the contributions from the target and projectile spin. The uncertainties in the $^4\text{He}+^{166}\text{Er}$ cross sections are about 10%, leading to 5% uncertainties in $\langle \ell \rangle$ derived from the sharp-cutoff model, $\langle \ell \rangle = \frac{2}{3} L_c$ where $\sigma_{\text{fus}} = (\pi/k^2)(L_c^2 + L_c)$.

E_{lab} (MeV)	E_x (MeV)	σ_{2n} (mb)	σ_{3n} (mb)	σ_{4n} (mb)	σ_{fus} (mb)	$\langle \ell \rangle$
			$^3\text{He}+^{167}\text{Er}$			
22	34.0	92±25	233±23	<40	365±50	5.4±0.3
25.1	37.2	120±30	437±44	159±16	716±60	6.9±0.4
27.2	39.1	91±25	310±31	254±60	655±70	6.8±0.4
			$^4\text{He}+^{166}\text{Er}$			
33.4	30.8	496	757	<40	1253	10.4
35.3	32.7	362	1088	<40	1450	11.5
38.6	35.9	199	1165	(60)	1424	12.0
40.0	37.3	163	1263	165	1591	12.9
43.1	40.3	120	969	498	1587	13.3
45.7	42.8	(70)	712	803	1585	13.7
48.1	45.2	(50)	446	947	1443	13.4
51.2	48.4	(40)	326	1051	1417	13.8

gamma rays emitted by evaporation residues. It was applied to all three systems studied. It is based on the use of a high-resolution Ge detector in combination with several NaI detectors. The Ge detector is used for tagging the different evaporation residues produced in the reaction. From the ratio of the coincidence to singles spectra, the value of M_γ for each channel (i) can be obtained as

$$M_\gamma^{(i)} = \frac{N_{\gamma i}^c(\text{tag})\eta}{N_{\gamma i}^s(\text{tag})\langle \epsilon_{\text{NaI}}^{(T)} \rangle}. \tag{1}$$

Here $N_{\gamma i}^c(\text{tag})$ and $N_{\gamma i}^s(\text{tag})$ denote the number of counts of the transition of interest in the coincidence and singles Ge detector spectra, respectively, for the transition being used as tag of this channel. $\langle \epsilon_{\text{NaI}}^{(T)} \rangle$ is the total efficiency of the combined NaI system, averaged over the gamma energy range (0.1 to 3 MeV) that spans the transitions

of interest. η is a correction factor to account for the coincidences produced in the NaI detectors by neutrons,[5] and has been taken as 0.9 based on the work of Sie et al.[6] Note that the multiplicities are independent of the Ge detector efficiency. The multiplicities are summarized in Table II.

A second experimental approach, involving the direct detection of evaporation residues after separation from beam particles, was used for the $^{16}\text{O}+^{154}\text{Sm}$ system. (The evaporation residues from the He-induced reactions do not have sufficient energy to escape from the target and be detected with reasonable efficiency.) One advantage of this technique is that it is essentially free of any channel bias. Evaporation calculations show that the widths of the recoil angular distributions differ by less than 15%, and any effect is weakened by the contributions of multiple scattering and charge state distributions. The latter effects depend only on atomic pro-
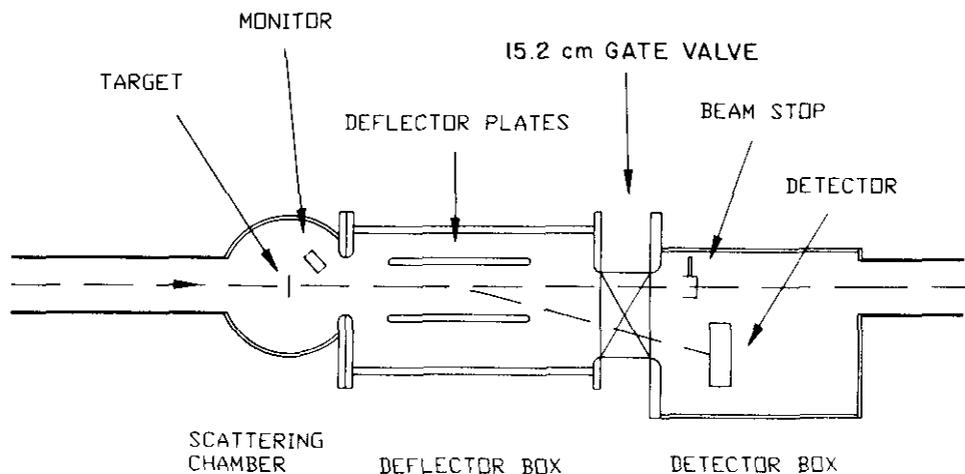

FIG. 2. Schematic view of the electrostatic deflector.

III. DEDUCTION OF MEAN ANGULAR MOMENTUM FROM GAMMA-RAY MULTIPLICITIES

In Fig. 4 we have plotted the results $M_\gamma^{(i)}$ for the three systems studied in this work as a function of the excitation energy of the compound nucleus. We have also plotted in this figure the $\langle \ell \rangle$ values deduced from the cross sections with the sharp-cutoff model. One sees that the multiplicities for the $^{16}O+^{154}Sm$ reaction are very comparable to those for the $^4He+^{166}Er$ reaction, confirming the usefulness of this reaction as a calibration reaction. One also notices that over most of the excitation energy range the multiplicities for the ^{16}O-induced reaction exceed that for the ^4He-induced reactions, demonstrating in
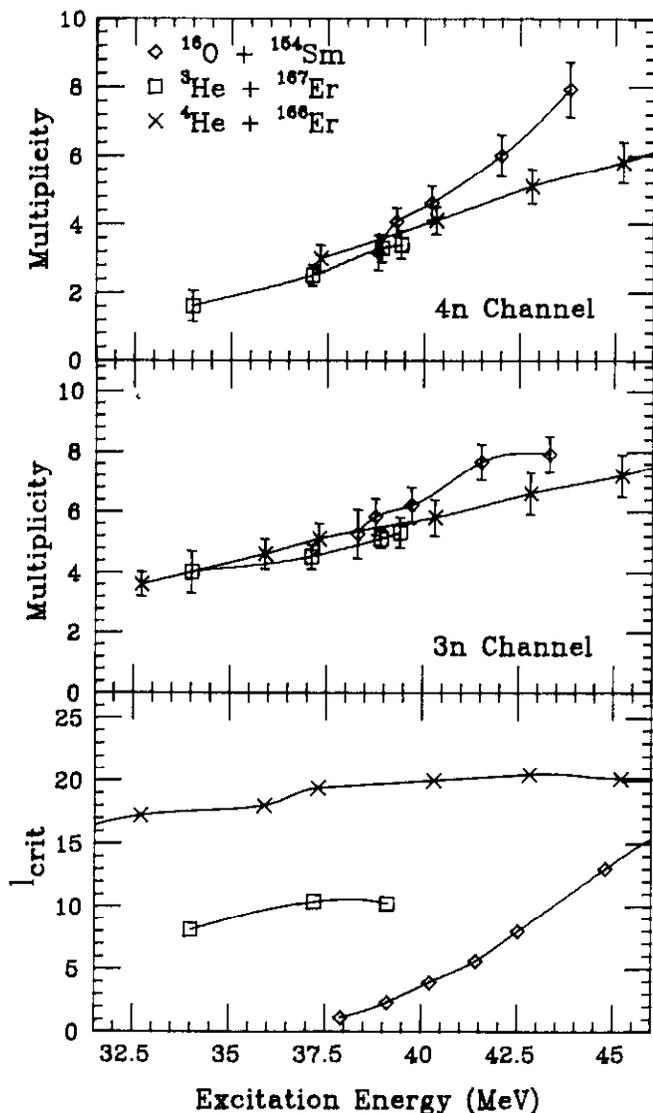

FIG. 4. Gamma-ray multiplicities as measured by the discrete gamma technique for the $3n$ (upper) and $4n$ (middle panel) channels as a function of excitation energy. The bottom panel shows the ℓ_{crit} values derived from the measured fusion cross sections (this work and Ref. 4).

a model-independent way that a lower limit to the mean angular momentum for the former reaction is larger than that deduced from $^4He+^{166}Er$ fusion cross sections using the sharp-cutoff approximation.

Gamma-ray multiplicities have long been used to infer information about the mean angular momentum of excited nuclei. Often the conversion from multiplicity to angular momentum is accomplished using simple relations of the form

$$\langle \ell \rangle = a(M_\gamma - b). \tag{3}$$

The constants a and b are determined empirically from measured multiplicities for fusion reactions occurring at energies well above the Coulomb barrier where the average angular momentum can be inferred relatively unambiguously from measured fusion cross sections. The constant b in the above expression is interpreted as the number of "statistical" gammas emitted early in the cascade which carry off little angular momentum, and typical values are between 2 and 4. The constant a is the average angular momentum carried off by the nonstatistical gammas. Typical values of a are between 1.5 and 2, indicating dominant contributions from stretched quadrupole gammas. Angular momentum carried off by neutrons is absorbed into these constants empirically.

Although simple and probably adequate when there is a reasonably large amount of angular momentum, the above approach can have quantitative limitations at modest angular momentum and when specific channels dominate the gamma-ray cascade. In particular, it neglects the ground-state spin of odd-A nuclei and the differing contributions of dipole and quadrupole radiation in even-even as compared to odd-A nuclei. We have therefore felt compelled to calibrate our conversion relationship between multiplicity and angular momentum. It is possible to do this in a rather direct manner, as it is possible to make the same ^{170}Yb compound nucleus formed in the $^{16}O+^{154}Sm$ reaction by the above-barrier reaction $^4He+^{166}Er$. In the next subsection we describe the measurements associated with this calibration reaction. We have also made a less complete study of the $^3He+^{167}Er$ reaction, which turns out to be less useful because the amount of angular momentum brought in is appreciably less than in the heavy ion reaction of interest.

A. Discrete photon tagging

We have explored a number of empirical approaches for the conversion of multiplicity to angular momentum, and have adopted a procedure similar to that of Halbert et al.[2] This procedure gives a more faithful reproduction of the loss of sensitivity of multiplicity to angular momentum at low angular momentum. The relation assumed is

$$\langle \ell_i \rangle_{tag} = 2(M_\gamma^{(i)} + 1 + BB_i - \langle M_s^i \rangle) + \langle M_s^i \rangle \langle \Delta J_s \rangle + M_n \langle \Delta J_n \rangle + J_h(i), \tag{4}$$

where the first term describes the angular momentum

cesses and should be independent of *xn* channel. Our electrostatic deflector is shown in Fig. 2 and consists of three parts: a detector chamber, an electrostatic deflector box, and a scattering chamber. Each of these parts can be isolated from the rest of the system, enabling us to change targets and manipulate the particle detectors without compromising the conditioning of the deflector itself. The deflector plates are located at 18 cm from the target and are made of polished stainless steel. They are 5 cm high, 25 cm long, and 1.25 cm thick. The separation and orientation of the plates can be easily changed. The plates are located in a stainless-steel box designed to hold up to ± 70 kV. A turbo-molecular pump provides the vacuum to this module. The detector chamber contains a beam stop and a large-area particle detector, both of which can be moved without breaking the vacuum. The particle detector system consists of a position-sensitive Breskin counter[7] followed by a large-area solid-state detector. The Breskin counter provides a position and a timing signal and the solid-state detector gives the energy of the particles. This system, when operated with a pulsed beam, provides us with the energy and time of flight of the particles, which enabled us to separate the fusion products from the elastic and other direct reaction products. In our case we have used a 1-nsec-wide beam pulse with a period of 780 nsec. The time of flight of the recoils was of about 350 nsec. The cylindrical scattering chamber is 25 cm in diameter and 25 cm high and can accommodate several NaI detectors around it. There is a reentrant port enabling the placing of a Ge detector 3.2 cm from the target.

In Fig. 3 we show typical time-of-flight spectra in singles and in coincidence with the NaI detectors. The larger peak in the singles spectrum is associated with the beam-like particles. At low bombarding energies, when the fusion cross section is close to a few mb, the magnitude of the tail of this peak under the recoil peak is the main source of uncertainty in extracting the area of the recoil peak in the singles spectrum. Considerable improvement was achieved in reducing this tail by carefully tuning the beam so as to minimize the amount of beam hitting the collimators. The enhancement of the recoil peak in the coincidence spectrum, as compared to the beamlike peak, can readily be understood as arising from the larger M_γ associated with the fusion processes as compared with the inelastic, transfer, and quasielastic processes. Slit scattered and degraded beam particles have no coincident gamma rays.

The raw gamma multiplicities M_γ^D obtained using our electrostatic deflector were calculated in a manner similar to the discrete photon tag case, namely,

$$M_\gamma^D = \frac{N^c(\text{recoil})\eta}{N^s(\text{recoil})\langle\epsilon_{\text{NaI}}^{(T)}\rangle},\qquad(2)$$

where $N^c(\text{recoil})$ and $N^s(\text{recoil})$ are the areas of the recoil peak in coincidence with the NaI detectors and in the singles spectra, respectively. An important property of
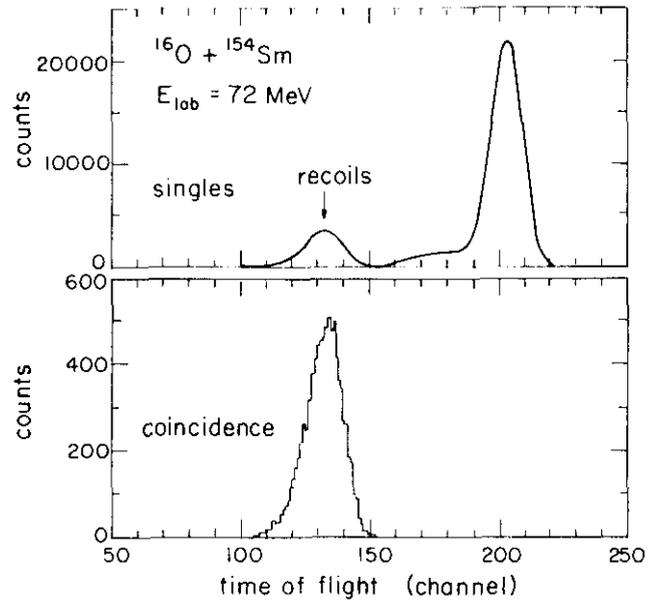

FIG. 3. Time-of-flight spectra for the system ^{16}O$+^{154}$Sm at $E_{\text{lab}}=72$ MeV, in singles and coincidence with the NaI detectors. Time increases to the left.

the multiplicities thus obtained is that they are independent of the efficiency of the electrostatic deflector. The results of these measurements are summarized in Table III.

TABLE II. Gamma-ray multiplicities measured in the present experiment. These "raw" values have not been corrected for gammas below the energy threshold or for internal conversion. The $\langle\ell^{\text{Ge}}\rangle$ values were obtained from Eq. (7).

E_{Lab} (MeV)	E_x (MeV)	$M_\gamma(3n)$	$M_\gamma(4n)$	$\langle\ell^{\text{Ge}}\rangle$
			^{3}He$+^{167}$Er	
27.5	39.4	5.3±0.5	3.4±0.4	6.8
27.0	38.9	5.1±0.3	3.3±0.4	6.8
25	37.1	4.5±0.4	2.5±0.3	6.9
22	34.0	4.0±0.7	1.6±0.45	5.4
			^{4}He$+^{166}$Er	
33.4	30.8	2.6±0.3		10.4
35.3	32.7	3.6±0.4		11.5
38.6	35.9	4.6±0.5		12.0
40.0	37.3	5.1±0.5	3.0±0.4	12.9
43.1	40.3	5.8±0.6	4.1±0.4	13.3
52.8	49.8	10.5±1.5	7.3±0.7	
			^{16}O$+^{154}$Sm	
61	38.8	5.2±0.6	3.1 ±0.4	9.2
61.5	39.3	5.8±0.5	4.1 ±0.2	10.0
62.5	40.2	6.2±0.4	4.6±0.2	10.9
64.5	42.0	7.6±0.5	6.0±0.2	13.4
66.5	43.8	7.9±0.6	6.2±0.2	13.3

TABLE III. M_γ^D obtained with electrostatic deflector using expression (2). $\langle \ell \rangle$ was obtained from expression (8).

E_{Lab} (MeV)	M_γ^D	ΔM_γ^D	$\langle \ell \rangle^D$
		^{16}O+^{154}Sm	
59.5	5.1	±0.5	9.9
60.5	5.7	±0.4	11.3
61.5	5.9	±0.3	12.0
62.5	6.0	±0.3	12.1
63.5	6.6	±0.3	13.55
64.5	6.9	±0.4	13.7
65.5	6.8	±0.3	13.0
67.5	8.1	±0.4	15.1
71.5	9.2	±0.1	16.2

with the mean compound nucleus spin given by

$$\langle \ell \rangle = \sum_i f_i [\ 2(M_\gamma^D + BB_i - \langle M_s^i \rangle)$$

$$+ \langle M_s^i \rangle \langle \Delta J_s \rangle + M_n^i \langle \Delta J_n^i \rangle]. \qquad (8)$$

The BB value for the 4n channel was taken as 0.9, and for the 3n channel values between 2.2 and 2.5 were used, depending on the bombarding energy. These values for deflector tagging are less than for discrete-photon tagging as one does not have the high-spin bias associated with the latter tag in the case of the 3n channel. We display the mean spin values obtained using the deflector together with those from the discrete-photon tagging technique in Fig. 6.

The present results give $\langle \ell \rangle$ values somewhat larger than obtained previously.[3] This is mostly due to inclusion of the 3n channel at the lowest energies where both the old and new studies overlap, but also reflects somewhat the new procedure for conversion of multiplicity to angular momentum. The small but apparently systematic tendency for the electrostatic deflector tagging to give higher $\langle \ell \rangle$ values than obtained in the new Ge detector tagging experiment is not understood, but the discrepancy is within the absolute uncertainties in measuring multiplicities and converting them to $\langle \ell \rangle$ values.

IV. MODEL COMPARISONS

We have previously published $\langle \ell \rangle$ values deduced from the earlier 4n channel tagging experiment.[3,5] At that time we compared the deduced $\langle \ell \rangle$ values with those calculated from the Wong model,[8] which assumes an ensemble of orientation-dependent parabolic one-dimensional barriers and averages over the random orientation of the target nucleus. There are basically four parameters in this model: the barrier height and curvature, the internucleon separation for the undeformed target, and the quadrupole deformation of the target nucleus. These parameters were constrained by fitting the fusion excitation function of Stokstad et al.[4] The deformation parameter

was taken as $0.22 \times 6.43 = 1.4$ fm based on the equivalent spheres analysis of Stokstad and Gross.[9] The internuclear separation was taken as $1.35(A_1^{1/3} + A_2^{1/3})$ on the basis of typical values obtained with realistic nuclear potentials. Finally, the barrier height and curvature energy ($V_B = 59.0$ MeV and $\hbar w = 3.5$ MeV) were obtained by fitting the fusion cross-section excitation function. The dependence of $\langle \ell \rangle$ on bombarding energy as calculated with this model is shown by the dashed line in Fig. 6. It is seen that this calculation underestimates $\langle \ell \rangle$ near and below the barrier.

We have also performed a coupled-channels calculation of $\langle \ell \rangle$ using the coupled-channels code CC DEF.[10] This code allows us to average over the random orientations of the deformed target nucleus and to include coupling to vibrational and transfer channels as well. Specifically we included the quadrupole and hexadecapole deformations ($\beta_2 R = 0.28 \times 6.43 = 2.44$ fm, $\beta_4 R = 0.07 \times 6.43 = 0.45$ fm) and the octupole vibration ($\beta_3 R = 0.10 \times 6.43 = 0.64$ fm) of ^{154}Sm. The β_2 value and the barrier height were adjusted to reproduce the excitation function as before. The β_2 value is somewhat larger than before but is closer to the value deduced from $B(E2)$ values by Raman et al.[11] The β_3 and β_4 values were taken from the literature.[12,13] The resulting $\langle \ell \rangle$ values are shown by the full curve in Fig. 6. The results of this calculation are in better agreement with experiment, although they still somewhat underestimate the $\langle \ell \rangle$ values in the vicinity of the barrier.

A tendency for theoretical calculations to underestimate the mean spin near the barrier has been noted in some but not all previous studies. A first attempt at systematizing the available data was made in 1988[14] and has been updated recently.[15,16] The preponderance of the available data suggests a failure of the existing models to completely account for the $\langle \ell \rangle$ values near and below the barrier. Additional work is required to elucidate the circumstances and origin of this discrepancy.

V. SUMMARY

We have extended our previous discrete gamma tagging measurement of $\langle \ell \rangle$ for the 4n channel of the ^{16}O +^{154}Sm reaction to include the 3n channel. Inclusion of the 3n channel leads to overall $\langle \ell \rangle$ values which are appreciably larger than before at the lowest bombarding energies. We have also developed a new tagging technique based on time-of-flight identification of the heavy residues after separation from the beam particles by an electrostatic deflector. This technique has allowed us to extend our measurements to lower energies and much lower cross sections. Comparison with models which include the shape degrees of freedom of the target nucleus lead to a qualitative understanding of the results. More quantitatively, the calculations underestimate somewhat the $\langle \ell \rangle$ values near and below the barrier.

carried away by stretched quadrupole nonstatistical gammas, the second term describes the (modest) amount of angular momentum carried off by the statistical gammas, and the third term accounts for angular momentum carried away by the evaporated neutrons. $J_h(i)$ is the angular momentum of the bandhead. The index i denotes the different evaporation residues produced in the reaction under study. $M_\gamma^{(i)}$ are the "raw" multiplicities obtained using expression (1). The $1+BB_i$ terms correct for the gamma in the tagging Ge detector and for transitions either too low in energy to be detected in the NaI or decaying by internal conversion. The BB_i values were estimated to be 0.9 for the $4n$ channel and 3.5 for the $3n$ channel. $\langle M_s^i \rangle$ and $\langle \Delta J_n \rangle$ were taken from the evaporation model code PACE as modified by Beene to employ a giant dipole resonance form for the $E1$ gamma strength function. The level density parameter employed ($a = A/8.5$) was determined from a fit to the xn channel yields. Typical values of $\langle M_s^i \rangle$ were 1.5–3, of $\langle \Delta J_s \rangle$ were 0.1–0.3, and of $\langle \Delta J_n \rangle$ were 0.1–0.3. It is interesting to note that these values were channel dependent, with M_s being larger for the $3n$ channel than for the $4n$ channel at energies where both channel yields were comparable.

We have extended the above procedure to take into account the fact that the discrete-photon tagging method only samples that part of the spin distribution that feeds the tagging transition. This biases the sample to higher spins, and a correction should be made for the contribution of the part of the spin distribution not sampled. This correction is most important for the $3n$ channel where the spin of the decaying state for the tag is $\frac{17}{2}$. This correction was estimated from statistical model calculations of the fractions of the spin distribution above J_i in the ith channel [$f_i(j < J_i)$], and below J_i [$f_i(j > J_i)$], where $J_i \rightarrow J_{i-2}$ is the tagging transition in this channel. For technical reasons these corrections were deduced from calculations from the evaporation code CASCADE.
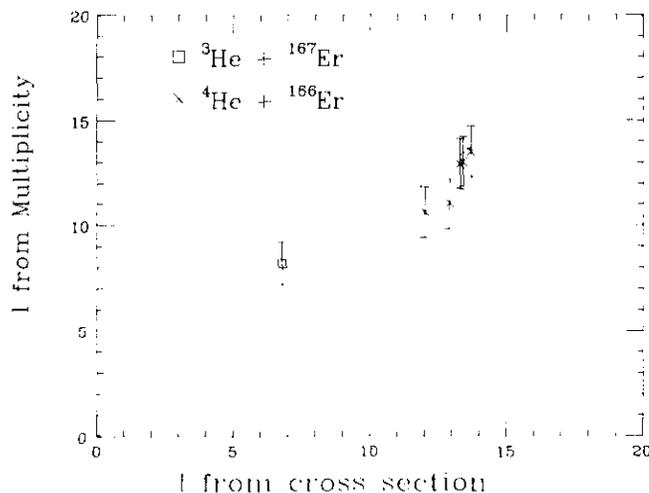
The mean spin of the distribution not sampled by the tagging was estimated to be $\frac{2}{3}$ the J_i of the tagging transition, an estimate that was confirmed by quantitative examination of the spin distribution for several sample cases.

This procedure can be summarized as follows. The $\langle \ell_i \rangle_{\text{tag}}$ values are deduced from Eq. (4) using experimental $M_\gamma^{(i)}$ values for each ith channel. The mean channel spin is then obtained from

$$\langle \ell_i \rangle = \frac{f_i(j < J_i)\frac{2}{3}J_i + f_i(j > J_i)\langle \ell_i \rangle_{\text{tag}}}{f_i(E)}, \qquad (5)$$

where

$$f_i(E) = f_i(j < J_i) + f_i(j > J_i) \qquad (6)$$

is the relative yield of the channel i at the bombarding energy E. The total mean angular momentum of the compound nucleus is obtained from

$$\langle \ell \rangle = \sum_i f_i \langle \ell_i \rangle. \qquad (7)$$

We first test the validity of this procedure by applying it to the $^4\text{He}+^{166}\text{Er}$ reaction where the mean angular momentum at each energy can be reliably known. The results of this procedure are shown in Fig. 5.

B. Deflector residue detection multiplicities

In this case the individual channel multiplicities are not known but the bias due to tagging on a transition not fed by the whole spin distribution is not present. The corrections for the modest amount of spin carried away by neutrons and statistical gammas are made as before,
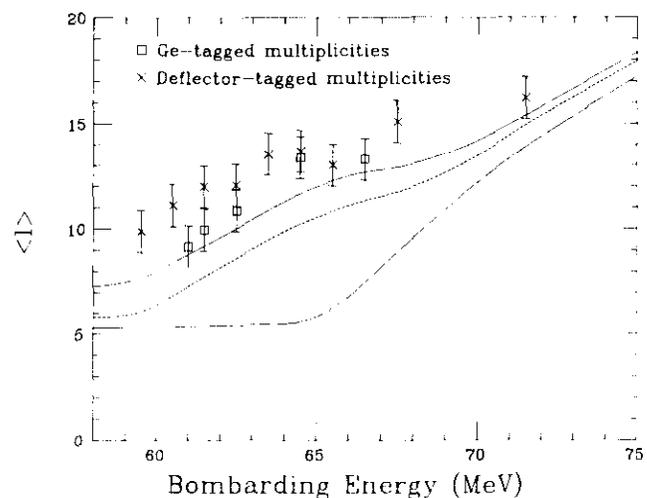

FIG. 6. Mean ℓ for $^{16}\text{O}+^{154}\text{Sm}$ as deduced from gamma-ray multiplicities determined by discrete gamma-ray and deflector-tagging techniques. The dashed and dash-dotted curves are from the Wong model with and without deformation. The full curve is from the coupled-channels calculation described in the text.

FIG. 5. Mean angular momentum derived from multiplicities versus mean ℓ derived from cross section for He-induced reactions.

*Present address: Dpto. de Física-TANDAR-CNEA—Buenos Aires, Argentina.

†Present address: Nuclear Physics Div. Bhabha Atomic Research Centre, Trombay, Bombay 400085, India.

[1] R. Vandenbosch *et al.*, Phys. Rev. Lett. **56**, 1234 (1986); **57**,1499 (1987).

[2] M.L. Halbert, J.R. Beene, D.C. Hensley, K. Honkanen, T.M. Semkow, V. Abenante, D.G. Sarantites, and Z. Li, Phys. Rev. C **40**, 2558 (1989).

[3] S. Gil, R. Vandenbosch, A. Lazzarini, and A. Ray, Phys. Rev. C **31**, 1752 (1985).

[4] R.G. Stokstad, Y. Eisen, S. Kaplanis, D. Pelte, U. Smilansky, and I. Tserruya, Phys. Rev. C **21**, 2427 (1980).

[5] R. Vandenbosch, B.B. Back, S. Gil, A. Lazzarini, and A. Ray, Phys. Rev. C **28**, 1161 (1983).

[6] S.H. Sie, J.O. Newton, and J.R. Leigh, Nucl. Phys. **A245**, 279 (1981).

[7] A. Breskin, R. Chechik, Z. Fraenkel, P. Jacobs, I. Tserruya, and N. Zwang, Nucl. Instrum. Methods **221**, 363 (1984).

[8] C.-Y. Wong, Phys. Rev. Lett. **31**, 766 (1973).

[9] R. G. Stokstad and E. E. Gross, Phys. Rev. C **23**, 281 (1981).

[10] J. Fernandez Niello, C. H. Dasso, and S. Landowne, Comput. Phys. Commun. **54**, 409 (1989).

[11] S. Raman *et al.*, At. Data Nucl. Data Tables **36**, 1 (1987).

[12] R. G. Helmer *et al.*, Nucl. Data Sheets **52**, 40 (1987).

[13] C.H. King *et al.*, Phys. Rev. C **20**, 2089 (1979).

[14] A. Charlop *et al.*, in *Proceedings of the Symposium on Heavy Ion Interactions Around the Coulomb Barrier, Legnaro, Italy, 1988*, edited by C. Signorini, S. Skorka, P. Spolare, and A. Vitturi (Springer-Verlag, Berlin, 1988), p.157.

[15] D.F. Digregorio *et al.*, in Workshop on the Interface between Nuclear Structure and Dynamics, Notre Dame, Indiana, 1990 (unpublished).

[16] R. Vandenbosch, Workshop on Heavy Ion Collisions at Energies Near the Coulomb Barrier, Daresbury, England, 1990 (unpublished).